Available online at www.sciencedirect.com
ScienceDirect
Geochimica et Cosmochimica Acta 70 (2006) 5883–5898
Geochimica
www.elsevier.com/locate/gca

Co-diagenesis of iron and phosphorus in hydrothermal sediments from the southern East Pacific Rise: Implications for the evaluation of paleoseawater phosphate concentrations

Simon W. Poulton [a,*], Donald E. Canfield [b]

[a] School of Civil Engineering and Geosciences, University of Newcastle upon Tyne, Drummond Building, Newcastle upon Tyne, NE1 7RU, UK
[b] Nordic Center for Earth Evolution (NORDCEE) and Institute of Biology, University of Southern Denmark, Campusvej 55, DK-5230 Odense, Denmark

Received 21 April 2005; accepted in revised form 11 January 2006

Abstract

We present a detailed study of the co-diagenesis of Fe and P in hydrothermal plume fallout sediments from ~19°S on the southern East Pacific Rise. Three distal sediment cores from 340–1130 km from the ridge crest, collected during DSDP Leg 92, were analysed for solid phase Fe and P associations using sequential chemical extraction techniques. The sediments at all sites are enriched in hydrothermal Fe (oxyhydr)oxides, but during diagenesis a large proportion of the primary ferrihydrite precipitates are transformed to the more stable mineral form of goethite and to a lesser extent to clay minerals, resulting in the release to solution of scavenged P. However, a significant proportion of this P is retained within the sediment, by incorporation into secondary goethite, by precipitation as authigenic apatite, and by readsorption to Fe (oxyhydr)oxides. Molar P/Fe ratios for these sediments are significantly lower than those measured in plume particles from more northern localities along the southern East Pacific Rise, and show a distinct downcore decrease to a depth of ~12 m. Molar P/Fe ratios are then relatively constant to a depth of ~35 m. The Fe and P speciation data indicate that diagenetic modification of the sediments is largely complete by a depth of 2.5 m, and thus depth trends in molar P/Fe ratios can not solely be explained by losses of P from the sediment by diffusion to the overlying water column during early diagenesis. Instead, these sediments are likely recording changes in dissolved P concentrations off the SEPR, possibly as a result of redistribution of nutrients in response to changes in oceanic circulation over the last 10 million years. Furthermore, the relatively low molar P/Fe ratios observed throughout these sediments are not necessarily solely due to losses of scavenged P by diffusion to the overlying water column during diagenesis, but may also reflect post-depositional oxidation of pyrite originating from the volatile-rich vents of the southern East Pacific Rise. This study suggests that the molar P/Fe ratio of oxic Fe-rich sediments may serve as a proxy of relative changes in paleoseawater phosphate concentrations, particularly if Fe sulfide minerals are not an important component during transport and deposition.

1. Introduction

The discharge of hydrothermal vent fluids rich in dissolved iron is a widespread feature of the global mid-ocean ridge system. The vent fluids rise buoyantly for tens to hundreds of metres, and subsequently form dilute, neutrally buoyant plumes which are laterally advected from the ridge crest by deep-ocean currents (e.g. Lupton and Craig, 1981; Reid, 1982; Baker et al., 1985). Upon mixing with alkaline oxic bottom-waters, a range of metal-rich sulfide, sulfate and (oxyhydr)oxide minerals precipitate from the acidic vent fluids (e.g. Feely et al., 1987, 1990a, 1992, 1994; Trocine and Trefry, 1988; Mottl and McConachy, 1990). Iron sulfide minerals precipitate rapidly (within a few seconds), whereas hydrous ferric oxides continue to precipitate for some time in the neutrally buoyant plume (Feely et al., 1992, 1996; Rudnicki and Elderfield, 1993). Most of the sulfide minerals are deposited close to the vent (Feely et al., 1987, 1994; Walker and Baker, 1988), but very fine-grained Fe sulfides may be retained with the colloidal

* Corresponding author.
E-mail addresses: s.w.poulton@ncl.ac.uk (S.W. Poulton), dec@biology.sdu.dk (D.E. Canfield).

0016-7037/$ - see front matter © 2006 Elsevier Inc. All rights reserved.
doi:10.1016/j.gca.2006.01.030

ferric oxide particles in the dispersing plume (Feely et al., 1987; Metz and Trefry, 1993). Prior to deposition, the hydrothermal particles may be transported for tens to hundreds of kilometres (Baker et al., 1985; Klinkhammer and Hudson, 1986).

The flux of Fe (oxyhydr)oxides derived from submarine hydrothermal sources is a relatively minor contributor to the global flux of Fe (oxyhydr)oxides to the marine environment (Canfield, 1998; Poulton and Raiswell, 2002). However, the enhanced reactivity of freshly precipitated hydrous ferric oxides, coupled with the fact that they form within the water column, means that they are very efficient scavengers of a variety of dissolved elements (e.g. P, As, V, Y, Be, REE) from seawater (e.g. Berner, 1973; Trocine and Trefry, 1988; Olivarez and Owen, 1989; Trefry and Metz, 1989; Feely et al., 1990a,b, 1991; German et al., 1990; Edmonds and German, 2004). In particular, this process exerts a major influence on the marine P cycle, and is estimated to remove 18–33% of the dissolved riverine P flux (Wheat et al., 1996).

The majority of P enrichment in hydrothermal plume particles occurs within the first few minutes of Fe (oxyhydr)oxide formation, primarily in the buoyant hydrothermal plume (Feely et al., 1992, 1994). Rudnicki and Elderfield (1993) suggest that the P enrichment occurs largely due to coprecipitation rather than adsorption, since only minimal scavenging of oxyanions occurs following the initial rapid precipitation of Fe (oxyhydr)oxides (German et al., 1991). This finds support in transmission electron microscope observations of thin-sectioned plume particles, which show a strong covariation of P and Fe over the entire particle section (Feely et al., 1990b), although this may also arise due to rapid adsorption at the oxide surface during progressive growth of the mineral phase. Nevertheless, regardless of the relative importance of coprecipitation versus adsorption, the extent to which P is scavenged has been shown to relate to the concentrations of particulate Fe and dissolved P, such that the molar P/Fe ratio in freshly precipitated particles behaves predictably on a global scale (Feely et al., 1998).

The predictable relationship between dissolved P and particulate Fe during hydrothermal scavenging has led to the suggestion that the molar P/Fe ratio may be a useful indicator of paleoseawater phosphate concentrations (Feely et al., 1998). This approach has been applied to banded iron formations to demonstrate low seawater phosphate concentrations during the Archean and early Proterozoic (Bjerrum and Canfield, 2002). The application of the P/Fe ratio to ancient sediments does, however, require that the ratio remains constant during particle transport and diagenesis. Hydrothermal sediments which remain oxic to depth in the sediment, and where iron reduction and associated P release is relatively minor due to the low organic contents, might be expected to preserve the depositional P/Fe ratio.

Few studies have directly investigated the preservation of P/Fe ratios in hydrothermal Fe (oxyhydr)oxide-rich deposits. Edmonds and German (2004) found that the P/Fe ratio in the Mid-Atlantic Rainbow hydrothermal plume was the same as in underlying short (up to 40 cm deep) cores, over a distance of 2–25 km from the source (Cave et al., 2002). By contrast, Schaller et al. (2000) found that the P/Fe ratio in a 2.5 m core located 34 km from the southern East Pacific Rise (SEPR) at ~10°S was approximately half that in SEPR plume particles from 13°S to 19°S (Feely et al., 1996). Thus the apparent preservational efficiency may vary, but the processes affecting the P/Fe ratio during diagenesis remain unclear.

Here we present a detailed investigation of the co-diagenesis of Fe and P in hydrothermal sediments from the western flank of the SEPR at ~19°S. The SEPR is one of the fastest spreading ridges on the global ridge-crest system and is characterised by frequent magmatic activity, resulting in extensive volatile-rich plumes (Feely et al., 1996; Ishibashi et al., 1997). Plume particles are predominately transported westwards to distances exceeding 1000 km from the ridge crest, resulting in sediments rich in hydrothermal Fe (oxyhydr)oxides even at the most distal sites (Dymond, 1981; Lupton and Craig, 1981). We have examined three sediment cores collected between 340 and 1130 km from the SEPR ridge crest during DSDP Leg 92. Chemical extraction techniques (Ruttenberg, 1992; Poulton and Canfield, 2005) were employed to evaluate changes in P and Fe speciation during diagenesis and with increasing distance from the ridge crest. The extraction procedure of Ruttenberg (1992) has been widely used to evaluate post-depositional changes in P speciation in marine sediments (e.g. Ruttenberg and Berner, 1993; Filippelli and Delaney, 1996; Eijsink et al., 2000; Schenau et al., 2000; Slomp et al., 2002; Van der Zee et al., 2002) but has not previously been applied to hydrothermal sediments. The increased information afforded by selective chemical extraction procedures provides valuable insight into the behaviour of P during diagenesis in oxic Fe-rich sediments, thus allowing further evaluation of the potential of the P/Fe ratio as an indicator of paleoseawater phosphate concentrations.

2. Study sites and methods

2.1. Core details

We sampled sediment cores collected during DSDP Leg 92 at Sites 598, 599 and 600 (Fig. 1). The cores were collected in 1983 and stored at 4 °C to prevent loss of moisture prior to sampling for the present study. To further ensure that the least altered sediment was analysed, the outer 1 cm of core was discarded. As detailed below, consistent trends in Fe mineral transformations are observed with sediment depth, suggesting that the data are not compromised by chemical alteration during storage.

Site details and sampled intervals are given in Table 1. Sedimentation rates were relatively low at all sites, ranging from 0.5 to 3.0 m/my over the sampled intervals (Lyle

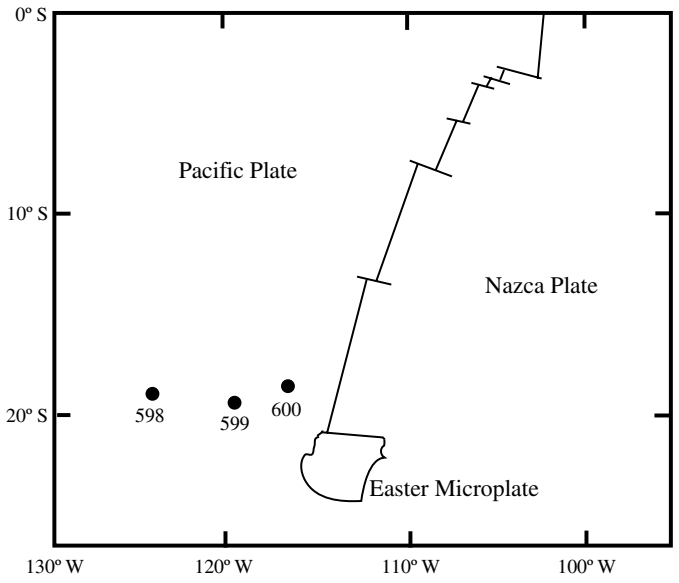

Fig. 1. Map showing site locations.

et al., 1986). Site 598 was sampled most intensively, with 50 samples over the uppermost 6 m (representing approximately 6 my of deposition). The top 10 cm of sediment at Sites 599 and 600 was sampled (5 samples for each core) in order to investigate possible variations in core geochemistry with distance from the rise crest.

Sites 598–600 of DSDP Leg 92 were chosen for this study partly because of a large quantity of available supporting data, including description of the general geochemistry (e.g. Lyle, 1986; Marchig and Erzinger, 1986). The sediments at all three sites are lithologically simple, composed primarily of hydrothermal precipitates derived from SEPR ridge crest vents, and carbonate (Lyle, 1986). The sediments also contain minor quantities of aeolian detrital material (Bloomstine and Rea, 1986), and trace quantities of phosphatic fish debris have been observed in some horizons (Marchig and Erzinger, 1986).

Organic matter contents in the three sediment cores are low, yielding minimal anoxic modification (Lyle et al., 1986). Thus, there is no evidence for the reductive mobilisation of Mn (Lyle et al., 1986), the most redox-sensitive of the common transition metals, and there is no apparent consumption of nitrate over the measured depth interval of 40 m (Gieskes and Boulégue, 1986). We can conclude that these sediments have remained oxic over the sampled intervals.

2.2. Analytical procedures

Iron speciation was determined using a modified version of the extraction procedure of Poulton and Canfield (2005). Extractant details and operationally defined target phases are given in Table 2. Three Fe pools were quantified; (1) Fe in the form of lepidocrocite and hydrous ferric oxides such as ferrihydrite (Fe_{HFO}), (2) Fe present as goethite and hematite (Fe_{goe}) and (3) silicate Fe (Fe_{sil}). The extractions used to estimate Fe_{HFO} and Fe_{goe} were performed sequentially, while Fe_{sil} was determined as the difference between total Fe (FeT) and the sum of the sequential phases; thus $Fe_{sil} = FeT - (Fe_{HFO} + Fe_{goe})$. XRD analyses revealed no evidence for lepidocrocite or hematite in these sediments, and thus Fe_{HFO} and Fe_{goe} consist primarily of hydrous ferric oxides and goethite, respectively (see also Marchig and Gundlach, 1982; Kastner, 1986). All Fe analyses were performed by flame atomic adsorption, and the reproducibility of each Fe extraction is given in Table 2. The total Fe technique dissolved >96% of the Fe from the PACS1 international sediment standard, and this efficiency is likely increased for hydrothermal sediments low in detrital silicate phases. Lyle (1986) reports XRF data for total Fe for subsamples of sediment from Site 598. These data are on average 8.4% higher than FeT data for a suite of the same samples measured by dissolution techniques (Dymond, 1981). Although direct comparison with our data is not possible, an examination of depth trends for FeT at Site 598 suggests that our FeT data are also somewhat lower than that of Lyle (1986), implying either a slight overestimation of total Fe by XRF in the presence of high concentrations of $CaCO_3$, or a slight underestimation by dissolution techniques.

Three different methods were used to determine the partitioning of P. The SEDEX method (Ruttenberg, 1992) quantifies five different P pools via a series of sequential extractions (Table 2). A single step in the extraction scheme of Schenau and De Lange (2000) was performed in order to determine concentrations of P associated with biogenic apatite (fish debris) plus carbonate (P_{bio}; Table 2). This method also extracts

Table 1
Site details and sampling intervals

Site	Location	Distance from ridge crest (km)	Interval sampled (cm)	Sedimentation rates		Sample age (my)
				Depth interval (m)	Rate (m/my)	
598	19°00′S, 124°04′W	1130	0–600	0–4.5	0.9	0–5.7
				4.5–6.8	3.0	
599	19°27′S, 119°53′W	640	0–10	0–1.5	1.3	0–0.08
600	18°56′S, 116°51′W	340	0–10	0–4.4	2.5	0–0.04

Sedimentation rates are based on the original age model given in Lyle et al. (1986), updated using the Lourens et al. (2004) scale.

Table 2
Summary of phosphorus and iron extractions, and the reproducibility of each stage

Phase	Symbol	Extractant	RSD (%)
SEDEX P method (Ruttenberg, 1992)			
1. Loosely bound + exchangeable P	P_{ex}	1 M $MgCl_2$ (pH 8): 2 × 2 h; water wash: 2 × 2 h	10.2
2. Iron-bound P	P_{Fe}	0.3 M Na-citrate/1 M $NaHCO_3$/0.14 M Na-dithionite: 8 h 1 M $MgCl_2$ (pH 8): 2 h; water wash: 2 h	9.2
3. Authigenic apatite + biogenic apatite + $CaCO_3$-bound P	P_{aut}	1 M Na-acetate (pH 4-acetic acid buffered): 6 h 1 M $MgCl_2$ (pH 8): 2 × 2 h; water wash: 2 h	7.6
4. Detrital apatite + other inorg. P phases	P_{det}	1 M HCl: 16 h	3.5
5. Organic P	P_{org}	Ashing at 550 °C: 2 h; 1 M HCl: 16 h	7.8
Total P	P_{tot}	Ashing at 550 °C: 8 h; near boiling 6 N HCl: 24 h	2.5
P (Schenau and De Lange, 2000)			
Exchangeable + $CaCO_3$-bound P + biogenic apatite (fish debris)	P_{bio}	2 M NH_4Cl (pH 7): 8 × 4 h	10.2
Fe and P (Poulton and Canfield, 2005)			
1. Hydrous ferric oxides + lepidocrocite	Fe_{HFO}	1 M hydroxylamine–HCl in 25% acetic acid (pH 2): 48 h; 1 M $MgCl_2$ (pH 8): 2 × 2 h	2.3
	P_{HFO}	Calculated as hydroxylamine–HCl soluble P − (P_{ex} + P_{aut})	4.0
2. Goethite + hematite	Fe_{goe}	0.35 M acetic acid/0.2 M Na-citrate/0.28 M Na dithionite: 2 h	1.9
	P_{goe}		6.6
Total Fe	FeT	Ashing at 550 °C: 8 h; near boiling 6 N HCl: 24 h	2.5

Relative standard deviation (RSD) was determined by replicate extractions (performed sequentially where appropriate) on hydrothermal sediment splits from the present study.

exchangeable P, and thus P_{bio} was determined as the difference between P determined via the Schenau and De Lange (2000) method and P_{ex} determined via the Ruttenberg (1992) method. Phosphorus was also determined in the Fe_{HFO} extract (Poulton and Canfield, 2005). This extraction dissolves P associated with hydrous ferric oxides, but also removes exchangeable P, carbonate-associated P and authigenic P. Thus, hydrous ferric oxide-associated P (P_{HFO}) = hydroxylamine-soluble P − (P_{ex} + P_{aut}). Goethite-associated P (P_{goe}) was determined as the difference between P_{Fe} (measured via the SEDEX procedure; Table 2) and P_{HFO}.

Phosphorus was measured on a UV–vis spectrophotometer as the phosphomolybdate-blue complex (Koroleff, 1976). The dithionite and citrate in the P_{Fe} extract interfere with the molybdate reagent, and thus P was measured in these samples after dilution to a citrate concentration of less than 2.4 mM (Yuan and Lavkulich, 1995; Eijsink et al., 2000). The reproducibility of each P extraction is given in Table 2. In a further check on the SEDEX procedure, the sum of the five sequential stages (P_{sum}) was compared to total P (P_{tot}) measured via a single 6 M HCl extraction on ashed samples. A plot of P_{sum} versus P_{tot} (not shown) gives a linear relationship ($r = 0.98$) with a slope of 0.88. Depth trends for our P_{tot} data for Site 598 are in close agreement with the XRF analyses of Lyle (1986).

Organic C was measured after a 12 h pre-treatment with 10% HCl at room temperature to remove carbonate phases. Carbonate C was determined as the difference between total C and organic C, measured on a Carlo Erba 1108 Elemental Analyzer. XRD analyses were performed on a Phillips PW1050 XRD with Cu Kα radiation.

3. Results and discussion

3.1. Evaluation of the hydrothermal component

Organic C (C_{org}) contents are very low throughout the sequence (Fig. 2), with an average value of 0.04 ± 0.02 wt% for Site 598 and values persistently less than 0.01 wt% for Sites 599 and 600 (data not shown for Sites 599 and 600, but all analytical data are presented in Appendix A). The low organic C contents are consistent with the low sedimentation rates and oxic bottom water conditions. Carbonate phases (C_{carb}) represent a substantial proportion of the sediment (Fig. 2), with an average $CaCO_3$ content of 76.4 ± 14.6 wt% for Site 598, varying between 42.8 and 94.2 wt%. Total Fe contents are also highly variable (ranging between 1.07 and 14.53 wt%) and depth profiles show a close inverse relationship with respect to C_{carb} (Fig. 2). Leinen (1986) suggests that these high amplitude variations in $CaCO_3$ are due to temporal variations in $CaCO_3$ deposition throughout the Pacific, rather than due to variations in the depositional flux of the hydrothermal component. Carbonate concentrations are relatively constant over the sampled intervals (0–10 cm) at Sites 599 (93.3 ± 1.0 wt%) and 600 (95.6 ± 0.5 wt%).

Aluminium is not enriched in hydrothermal particulates (German et al., 1991), and thus detrital inputs may be calculated from the pelagic deep sea sediment ratio of each element to Al [$(X/Al)_{ds}$] and the Al contents (utilizing Al data reported in Lyle, 1986 and Marchig and Erzinger, 1986) of the SEPR sediments (e.g. Cave et al., 2002):

$$[X]_{detrital} = (X/Al)_{ds} \times [Al]_{total} \quad (1)$$

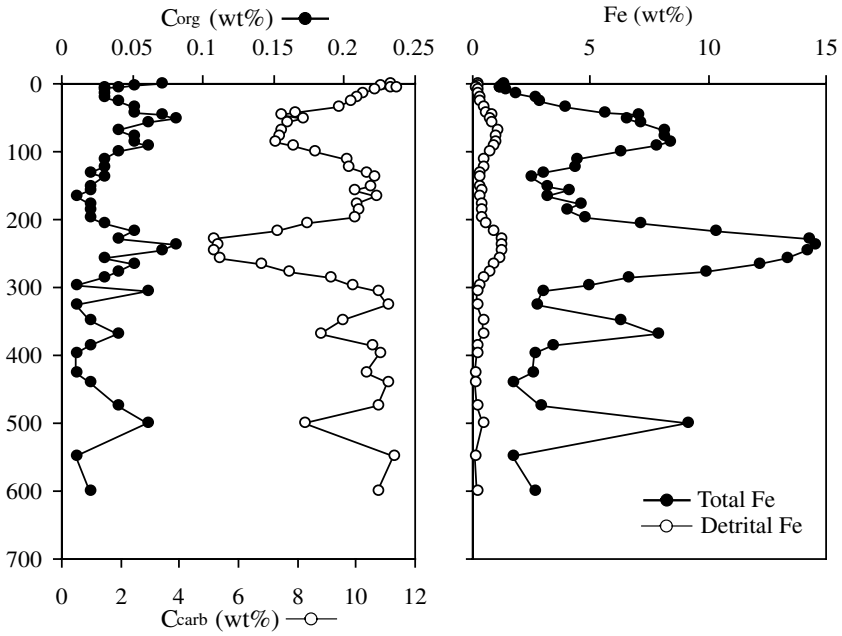

Fig. 2. Depth profiles for C_{org}, C_{carb}, total Fe, and detrital Fe at Site 598.

Table 3 summarises the average detrital elemental inputs to each core and details the pelagic deep sea sediment compositions used to calculate these inputs. Detrital inputs are relatively low at all sites, consistent with the previously reported dominance of hydrothermal inputs to these sediments (Lyle, 1986). However, detrital inputs are not uniform with depth (Fig. 2) and thus total Fe and P concentrations are corrected for the specific detrital inputs of these elements to each sample horizon.

3.2. Iron speciation

Ferrihydrite is a relatively unstable mineral under most environmental conditions, and Fig. 3 shows a progressive transformation to the more stable mineral form of goethite during burial of hydrothermal precipitates (the speciation of Fe in detrital sediments supplied to these sediments is unknown, and thus no attempt has been made to correct speciation data for detrital Fe inputs). Under oxic conditions, the formation of goethite from ferrihydrite involves the dissolution of ferrihydrite, followed by nucleation and growth of goethite from solution via the monovalent Fe(III) ions $Fe(OH)_2^+$ and $Fe(OH)_4^-$ (Schwertmann and Murad, 1983). At the pH of seawater, a solid state transformation to hematite is favoured over the formation of goethite (Schwertmann and Murad, 1983). However, the presence of certain elements (e.g. Ti) may enhance the formation of goethite over hematite (Fitzpatrick et al., 1978).

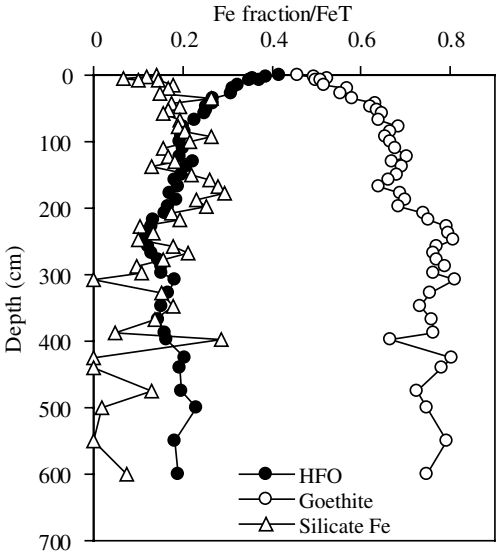

Fig. 3. Chemical partitioning of Fe at Site 598.

Table 3
Element concentrations in pelagic deep sea sediments and the average detrital contents of each element in cores 598, 599 and 600

Element	Deep sea clay composition (ppm)	Core 598 av. detrital proportion (% $[X]_{total}$)	Core 599 av. detrital proportion (% $[X]_{total}$)	Core 600 av. detrital proportion (% $[X]_{total}$)
Al	97,000[a]			
Fe	60,000[a]	7.0	9.1	10.4
P	1,500[b]	5.7	6.5	5.8

Detrital proportions are reported relative to the total concentration of each particular element ($[X]_{total}$).
[a] Kyte et al. (1993).
[b] Turekian and Wedephol (1961).

Variations in silicate Fe are controlled to a certain extent by the relative proportions of aeolian sediments supplied to each horizon. Also possible is the formation of Fe containing clays at the expense of ferrihydrite (reverse

weathering), which may be responsible for the downcore increase in Fe_{sil} over the top 30 cm (e.g. Curtis, 1985; Michalopoulos and Aller, 1995; Ku and Walter, 2003).

The transformation of ferrihydrite to more stable mineral forms can occur over a few days to weeks under certain conditions, but the coprecipitation of transition metals and oxyanions within the ferrihydrite crystal structure retards the transformation (Zhao et al., 1994; Cornell and Schwertmann, 1996). Furthermore, Kennedy et al. (2004) have shown that hydrothermal ferrihydrite deposits may be stabilized by bacteria, and attributed this to restricted crystal growth due to microbial surface functional groups. Our chemical extraction results provide support for both a relatively slow rate of ferrihydrite conversion (Fig. 3 and see below), and the long-term stabilization of a proportion of the hydrothermal ferrihydrite, as the transformation to goethite apparently ceases at a depth of about 250 cm (Fig. 3).

Since the transformation of ferrihydrite to goethite involves a dissolution phase, there is significant potential for the release of scavenged P to solution. This could occur both during diagenesis and during transport in the water column, and the ultimate fate of P released in these two circumstances may be very different. An equation for the overall ferrihydrite transformation rate *during diagenesis* can be written in the form:

$$-\frac{\mathrm{d}(\mathrm{Fe_{HFO}/FeT})}{\mathrm{d}t} = k(\mathrm{Fe_{HFO}/FeT})^a \quad (2)$$

where a is the reaction order with respect to the proportion of ferrihydrite transformed (relative to total Fe, expressed as a percentage), and k is the rate constant ($\mathrm{my^{-1}}$). A plot of $\ln(\mathrm{Fe_{HFO}/FeT})$ versus time over the top 250 cm at Site 598 (i.e. the zone where ferrihydrite transformation occurs; Fig. 3) is approximately linear (Fig. 4), indicating that the reaction is first order with respect to the proportion of total Fe present as ferrihydrite. The slope of the linear relationship in Fig. 4 gives a value for the rate constant, k, of $0.299 \pm 0.009\ \mathrm{my^{-1}}$. The half life ($t_{1/2}$) for the transformation of ferrihydrite can then be calculated using Eq. (3):

$$t_{1/2} = \ln(2)/k \quad (3)$$

This gives a half life of 2.32 ± 0.07 my, indicating a rather slow rate of transformation during diagenesis.

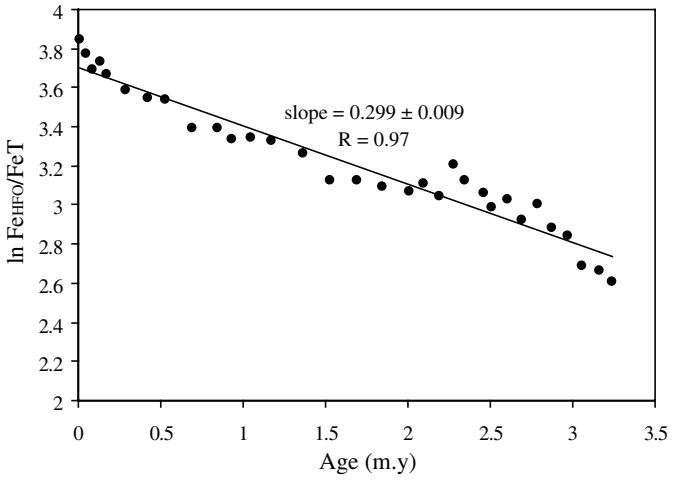

Fig. 4. Proportion of ferrihydrite transformed to other mineral phases (calculated relative to total Fe) as a function of sediment age.

Whether this half life can be directly applied to the transformation rate during transport in the hydrothermal plume is unclear. Nevertheless, it is instructive to consider the calculated half life in relation to possible transport times for particulates in the hydrothermal plume. At present, direct measurements of current velocities at distal plume sites along the SEPR are lacking. However, current velocities of 0.2–3 cm $\mathrm{s^{-1}}$ have been measured in the Labrador Sea (Speer et al., 1999), and the North Atlantic Current averages 3–4 cm $\mathrm{s^{-1}}$ over the Mid-Atlantic Ridge (Bower et al., 2002). Lupton et al. (1998) also report an average particle velocity of 2.4 cm $\mathrm{s^{-1}}$ during a major hydrothermal event on the north Pacific Gorda Ridge, and Bertram et al. (2002) measured an average on-axis current velocity of 1.6 cm $\mathrm{s^{-1}}$ near the Main Vent field on Endeavour Ridge. Assuming a current velocity for the SEPR plume in the range of 0.2–4 cm $\mathrm{s^{-1}}$, plume particles could take between several months to 16 years to be transported distances of over 1000 km. This would suggest that, in order to exert any significant impact on particle geochemistry, the transformation rate for ferrihydrite during transport in the water column would need to be many orders of magnitude higher than in the sediment.

3.3. Phosphorus diagenesis

The use of the P/Fe ratio as an indicator of paleoseawater phosphate concentrations depends on the extent of P mobilisation during diagenesis and on the processes affecting P retention within the sediment. The chemical partitioning of phosphorus provides some insight into these processes, and in Fig. 5 phase associations are shown normalised to total P (to account for depth variations in the depositional flux of carbonate relative to Fe oxides and associated P). Detrital P is a minor component throughout Site 598 ($3.4 \pm 1.7\%$ of P_{tot}), consistent with the low detrital inputs to these sediments (Lyle, 1986; Marchig and Erzinger, 1986). Organic-bound phosphorus also represents only a minor proportion of total P ($P_{org} = 0.7 \pm 0.4\%$ of P_{tot}) due to the low organic C contents (Fig. 2). Nevertheless, there is a distinct downcore decrease in P_{org} towards zero at depth, indicating the release of organic P to solution during organic matter diagenesis.

There are three main sediment sinks for the phosphorus released during ferrihydrite dissolution and organic matter diagenesis, and these are apparently established close to the sediment–water interface (as evidenced from the relatively constant P speciation profiles below ~50 cm depth; Fig. 5). Firstly, P may be readsorbed at the Fe (oxyhydr)oxide surface. Exchangeable P is only a minor sink for P in these sediments ($P_{ex} = 1.3 \pm 0.9\%$ of P_{tot} in core

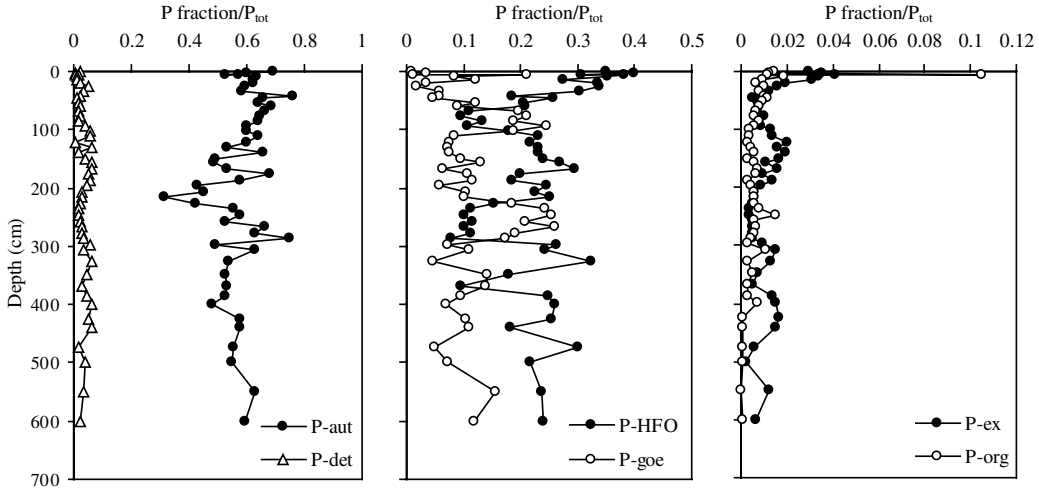

Fig. 5. Chemical partitioning of P at Site 598.

598), however, the extent to which *exchangeable* P may provide an adequate measure of the total *adsorbed* P pool is unclear. At best, the operationally defined extraction to determine exchangeable P probably somewhat underestimates total adsorbed P. Nevertheless, any original exchangeable P will be almost entirely released to solution during the initial dissolution of the ferrihydrite surface. However, some exchangeable P is buried below a depth of about 250 cm (Fig. 5), where the transformation of ferrihydrite to goethite ceases (Fig. 3). This suggests that a small fraction of the P released to solution is ultimately readsorbed and buried in association with the Fe (oxyhydr)oxides.

The major sink for P released during diagenesis ($58.1 \pm 8.3\%$ of P_{tot}) is via incorporation into authigenic phases (Fig. 5), which include both apatite and P associated with carbonates (Table 2). However, the technique of Schenau and De Lange (2000) provides an estimate of exchangeable P plus $CaCO_3$-bound P plus biogenic apatite (fish debris; Table 2). Concentrations of P associated with biogenic apatite and $CaCO_3$ (i.e. after subtraction of exchangeable P as measured by the SEDEX procedure) are low at all horizons ($1.0 \pm 0.8\%$ of the total P content at Site 598; see Appendix A), suggesting that authigenic apatite is the major sink for P in these sediments. The formation of significant concentrations of authigenic apatite has not previously been demonstrated during diagenesis of hydrothermal sediments, but is consistent with the observed formation of authigenic carbonate fluorapatite during diagenesis in many continental margin and deep sea sediments (e.g. Ruttenberg and Berner, 1993; Lucotte et al., 1994; Filippelli and Delaney, 1996; Eijsink et al., 2000; Van der Zee et al., 2002).

A large proportion of the phosphorus also occurs in association with Fe (oxyhydr)oxides ($P_{Fe} = 27.3 \pm 5.3\%$). P_{HFO} and P_{goe} depth profiles show some scatter (Fig. 5), but there is a clear overall decrease in P_{HFO} and a concomitant increase in P_{goe} over the upper portion of sediment at Site 598, as scavenged P is released to solution following ferrihydrite dissolution and subsequently co-precipitated in association with secondary goethite. Below a depth of ~50 cm the P_{HFO} fraction accounts for $19.7 \pm 6.7\%$ of P_{tot}, while the P_{goe} fraction accounts for $13.1 \pm 6.2\%$ of P_{tot}. Furthermore, the average molar P_{goe}/Fe_{goe} ratio (0.014 ± 0.009) for Site 598 is considerably lower than the average molar P_{HFO}/Fe_{HFO} ratio (0.064 ± 0.023) (Fig. 6), and thus coprecipitation of P during goethite formation is clearly less efficient, per mass of Fe, than P scavenging by ferrihydrite in the hydrothermal plume.

The fact that the redistribution of P is largely complete within the upper 50 cm of sediment (Fig. 5) implies a relatively rapid transformation rate during diagenesis. This contrasts with the Fe speciation data, whereby the

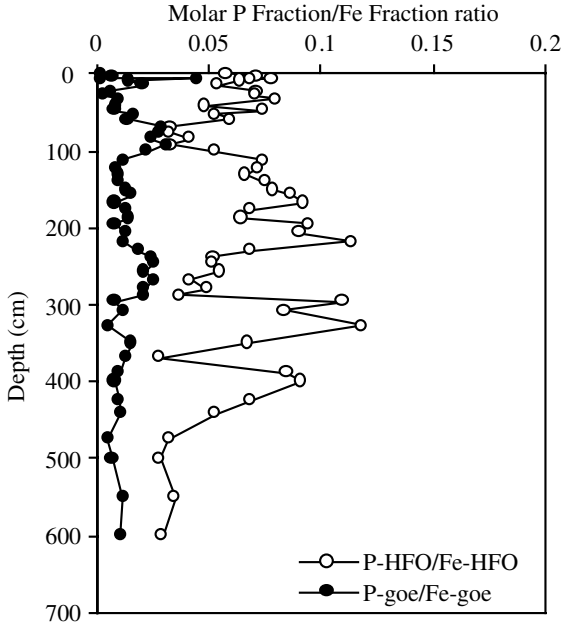

Fig. 6. Molar P_{HFO}/Fe_{HFO} and P_{goe}/Fe_{goe} ratios at Site 598.

transformation of ferrihydrite to more stable mineral forms apparently continues to a depth of around 250 cm (Fig. 3). However, by a depth of 50 cm approximately 75% of the original ferrihydrite has been transformed to more stable mineral forms, and this increases to only around 85% at depth. Any P released during ferrihydrite dissolution between 50 and 250 cm depth will presumably be largely partitioned between the P_{aut} and P_{goe} pools, but the P speciation techniques employed here may not be sufficiently accurate to identify this relatively small amount of redistributed P.

The rates of P transformation are clearer when comparing the average proportions of P_{Fe} and P_{aut} over the top 10 cm at Sites 598–600, since the surficial sediments at Site 600 are considerably younger than those at Sites 598 and 599 (Table 4). Thus, as observed in organic-rich marine sediments (e.g. Ruttenberg and Berner, 1993; Filippelli and Delaney, 1996), the relative importance of the P_{aut} fraction increases with age (Table 4). However, in the case of these hydrothermal sediments, the increase in the P_{aut} pool obviously occurs largely at the expense of the P_{Fe} pool, in contrast to organic-rich sediments, where a significant proportion of the P may be supplied by organic matter degradation (e.g. Ruttenberg and Berner, 1993; Filippelli and Delaney, 1996).

3.4. Molar P/Fe ratios

Molar P/Fe ratios for Sites 598–600 are shown in Fig. 7A. The molar P/Fe ratio for Site 598 shows a distinct downcore decrease from values averaging 0.10 ± 0.01 over the top ten cm, to values of ~0.06 at 600 cm depth. Average values over the top ten cm at Sites 599 and 600 are slightly lower than for this interval at Site 598, with both cores averaging 0.08 ± 0.02. The average surficial molar P/Fe ratios for Sites 598–600 are 40–50% lower than the average of 0.17 ± 0.02 reported for freshly precipitated particles from the SEPR hydrothermal plume (Feely et al., 1996). This implies a significant loss of scavenged P from the distal hydrothermal sediments, provided the SEPR plume particles analysed by Feely et al. (1996) between 13°33′ and 18°40′S are equivalent to distal particles at 19°S. This apparent P loss from surficial sediments is similar to that reported for sediments deposited 34 km from the SEPR at ~10°S (Schaller et al., 2000), but contrasts with an apparent complete retention of P beneath the Mid-Atlantic Rainbow hydrothermal plume (Edmonds and German, 2004).

Table 4
Average P_{Fe}/P_{tot} and P_{aut}/P_{tot} ratios for the top 10 cm of cores 598, 599 and 600, and correlation coefficients (r^2) obtained for the linear relationships of these parameters with average sediment age over this depth interval

Site	Age (my)	P_{Fe}/P_{tot}	P_{aut}/P_{tot}
598	0.052	0.334 ± 0.099	0.603 ± 0.064
599	0.035	0.374 ± 0.055	0.518 ± 0.064
600	0.018	0.473 ± 0.050	0.361 ± 0.045
r^2		0.94	0.97

The continued decrease in the molar P/Fe ratio throughout the sampled interval at Site 598 (Fig. 7A) is perhaps surprising. The data-set of Lyle (1986), going to greater depth, shows that this decrease continues to around 12 m (Fig. 7B). Below this depth the ratio remains relatively constant at 0.024 ± 0.004 to a depth of around 35 m, where it becomes highly variable but with an overall increase. Our Fe and P speciation data provide clear evidence that diagenetic modification of Fe and P partitioning is largely complete by 2.5 m below the sediment–water interface. Further loss of P from the sediment below a depth of 2.5 m would require the extremely unlikely scenario of P release from ferrihydrite without any mineralogical transformation, and without any subsequent trapping of P in authigenic phases or by readsorption onto Fe (oxyhydr)oxides during diffusion towards the sediment–water interface. Thus, the continued decrease in the molar P/Fe ratio to a depth of ~12 m is unlikely to be solely due to release of scavenged P during ferrihydrite dissolution, with subsequent loss of P by diffusion to the overlying water column. In the discussion below we attempt to reconcile the apparent paradox between the Fe and P speciation data, and depth trends in molar P/Fe ratios.

3.5. Synthesis

The two main aspects of the data that require further consideration in the context of this study are the lower ratios in surficial sediments relative to plume particles at the ridge crest, and the continued decrease in molar P/Fe ratios to a depth of ~12 m (Fig. 7). One explanation for the lower P/Fe ratios in deposited sediments relates to P losses by diffusion from the sediment during ferrihydrite transformations and organic matter diagenesis close to the sediment-water interface. As highlighted above, a maximum diffusional loss of 40–50% of P is indicated in surficial sediments from the three sediment cores.

A second potential explanation for the low molar P/Fe ratios relates to the behaviour of hydrothermal pyrite. Pyrite is a relatively inefficient scavenger of oxyanions such as phosphate, and the region to the south of 17°20′S on the SEPR is characterised by the highest discharges of H_2S yet seen on the global ridge crest system (Urabe et al., 1995; Feely et al., 1996). This results in high S/Fe ratios in the plume particles (0.5–4.1) relative to those found at more northern sites (S/Fe = ~0.18). The larger sulfide minerals formed by reaction with H_2S in ascending hydrothermal plumes are deposited close to the vent, but the finest sulfides (particularly pyrite) may be transported away from the vents in the neutrally buoyant plume (Feely et al., 1987; Walker and Baker, 1988). In situ dissolution studies with pure sulfide minerals at the southern Juan de Fuca Ridge, suggest that fine-grained pyrite (2 μm diameter) may be completely oxidised in 100–200 days (Feely et al., 1987). As discussed above, the available data suggest that plume

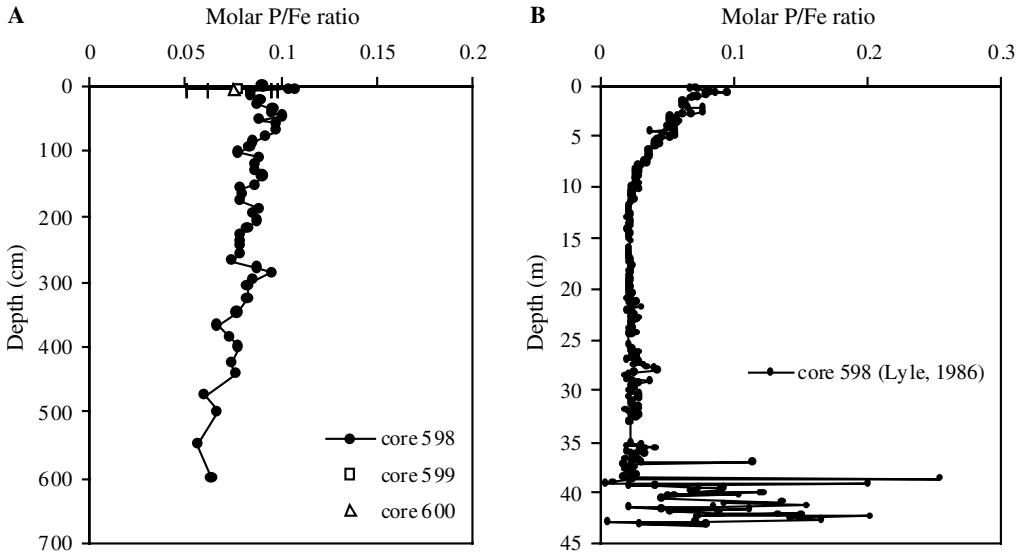

Fig. 7. Molar P/Fe ratios. (A) Data from the present study for Sites 598, 599 and 600 (corrected for detrital inputs and biogenic P additions). Data for the top 10 cm of Sites 599 and 600 are plotted as averages, where the error bars represent 1 standard deviation. (B) Data for Site 598 (corrected for detrital inputs but not biogenic P additions) from Lyle (1986).

particles likely take between several months to 16 years to be transported distances of over 1000 km. Thus we can not rule out the possibility that fine-grained pyrite may be transported considerable distances in the SEPR hydrothermal plume prior to deposition. Once deposited, pyrite will continue to be oxidised, but secondary Fe (oxyhydr)oxides will only be able to scavenge P from the surrounding porewater, resulting in relatively low P/Fe ratios. Some of the SEPR plume particles analysed by Feely et al. (1996) were measured at sites with relatively high sulfide contents, but the exact source and composition of the particles supplied to the distal sites of the present study are unknown. Thus, the source plume particles may have been particularly rich in pyrite, and therefore, oxidation of pyrite during diagenesis could potentially account for some, if not all, of the apparent loss of P in deposited SEPR sediments. Schaller et al. (2000) discount the possibility that pyrite oxidation could be responsible for the 50% loss of P in deposited SEPR sediments relative to plume particles, based on the low total S contents of the deposited sediments. However, there is no reason to assume that the solid phase S contents of oxidised hydrothermal sediments will reflect the original pyrite content, since a large proportion of the sulfate produced during oxidation may diffuse out of the sediment.

Pyrite oxidation following deposition also provides a potential explanation for the contrasting extent of preservation of the plume particle P/Fe ratio in deposited SEPR sediments (this study; Schaller et al., 2000) relative to Mid-Atlantic Rainbow sediments (Edmonds and German, 2004). The Rainbow hydrothermal plume is characterised by very low S/Fe ratios (0.04; Douville et al., 2002), and thus pyrite oxidation would not be expected to exert a strong influence on the molar P/Fe ratio of deposited sediments.

We now consider possible explanations for the continued decrease in molar P/Fe ratios below the apparent depth of active diagenetic modification (Fig. 7). Two processes may potentially contribute to the observed depth trends: (1) chemical modification of the plume particles during transport, and (2) temporal variations in SEPR dissolved P concentrations. Feely et al. (1992) found that the molar P/Fe ratio in neutrally buoyant plume particles from the Juan de Fuca Ridge was essentially constant over distances of around 100 km from the ridge crest. Edmonds and German (2004) similarly found that the P/Fe ratio in Rainbow hydrothermal plume particles behaved conservatively over a distance of up to 25 km from the ridge crest. Other scavenged elements, such as V and As, have also been shown to exhibit constant ratios to Fe during transport in the neutrally buoyant plume (e.g. Feely et al., 1992; Edmonds and German, 2004). These observations find support in laboratory studies of scavenged V and As, where constant ratios to Fe were observed for more than 80 days in hydrothermal particulates stored in unamended seawater sampled from vent plumes on the Mid-Atlantic Ridge (Metz and Trefry, 1993). These studies clearly suggest that, once formed, the hydrothermal particle P/Fe ratio is not generally altered by subsequent adsorption/desorption processes.

Temporal changes in dissolved P concentrations off the SEPR may also be invoked as a potential explanation for the molar P/Fe trends. Highly variable P/Fe ratios are observed in sediments deposited 16.5–15 my ago at Site 598 (Fig. 8), which Lyle (1986) suggests may be due to rapid fluctuations in dissolved P, although this could also be accounted for by inconsistency in the hydrothermal component at this time. A relatively wide degree of variability then persists until ~13 my ago, followed by relatively

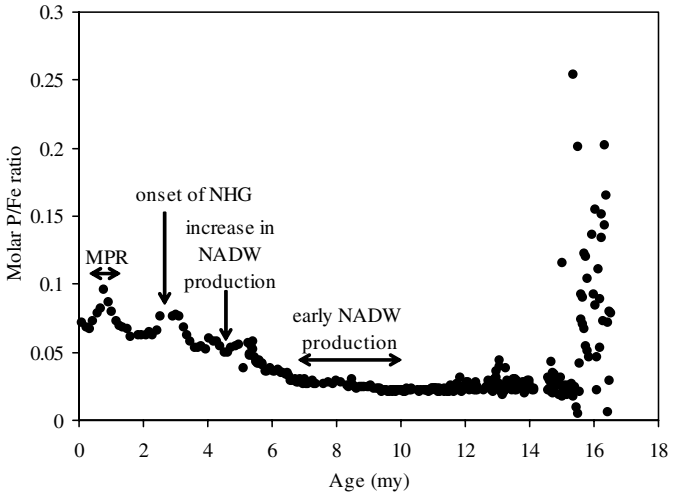

Fig. 8. Molar P/Fe ratios (corrected for detrital additions) for Site 598 as a function of sediment age. Chemical data are from Lyle (1986). MPR, Mid-Pleistocene Revolution; NHG, Northern Hemisphere Glaciation; NADW, North Atlantic Deep Water.

constant P/Fe ratios between 13 and 10 my. Between 10 and 6.5 my there is a small gradual rise in P/Fe, followed by a more dramatic rise over the last 6.5 my. Superimposed on these trends are periods, particularly over the last 5–6 my, where the molar P/Fe ratio exhibits pronounced peaks and troughs.

The history of seawater phosphorus during the Cenozoic is widely debated. The primary source of P to the oceans is via rivers, which transport P produced from continental weathering (e.g. Froelich et al., 1982; Filippelli and Delaney, 1994). In one model, increased global silicate weathering rates over the Cenozoic, often attributed largely to a gradual acceleration in erosion rates on the Himalaya-Tibetan plateau since collision, are taken to indicate increased fluxes of P to the oceans (e.g. Raymo and Ruddiman, 1992; Raymo, 1994). However, changes in P input need not necessarily result in increased dissolved P concentrations, since any change in the input flux of P would likely be matched by a change in P export to sediments (which on a global scale is predominantly in the form of organic P). Thus, phosphorus accumulation rates determined from a range of environments and over periods considerably longer than the residence time of P in the ocean (16–38 ka; Ruttenberg, 1993) are commonly used to reconstruct changes in P input to the ocean (see Delaney and Filippelli, 1994; Filippelli and Delaney, 1994; Föllmi, 1995). However, such studies have produced conflicting results. Föllmi (1995) compiled a global dataset of phosphorus accumulation rates from various paleoceanographic and sedimentological settings, and suggested that P accumulation rates have increased over the last 32 my, with a particularly rapid increase over the last 7 my. This was suggested to be a response to the onset of major glaciation rather than directly due to increased erosion rates on the Himalaya-Tibetan plateau. However, based on P accumulation rates in eastern equatorial Pacific sites it has been suggested that there is little evidence for increasing P fluxes during the Cenozoic (Delaney and Filippelli, 1994; Filippelli and Delaney, 1994). Furthermore, organic carbon burial rates are generally considered to have decreased over the last 15–20 my, whereas increased import of P from continental weathering would be expected to result in increased organic carbon production and burial (see Delaney and Filippelli, 1994).

An alternative explanation for the variations in molar P/Fe ratios relates to the redistribution of nutrients between the Atlantic and Pacific. Nutrient distribution in the ocean is controlled by a balance between deep water circulation and biological activity. The North Atlantic is the most significant area of deep water formation, and North Atlantic Deep Water (NADW) flows south into the Antarctic Circumpolar Current (ACC) (Broeker and Peng, 1982). The ACC then transports NADW and Antarctic Bottom Water (AABW) into the Pacific and Indian ocean basins (Reid and Lynn, 1971), resulting in a steady push of nutrients to these areas. It has been suggested that NADW production has largely persisted over the last 14 my, and has been a major factor controlling the global thermohaline ocean circulation system and climate (Woodruff and Savin, 1989; Wright and Miller, 1996; Frank et al., 2002). There have, however, been significant changes in the intensity of NADW production over this period, and here we attempt to ascertain whether these changes, and hence redistribution of phosphorus between the Atlantic and Pacific, are reflected in the molar P/Fe record at Site 598.

The closure of the Panama gateway has been suggested to be the most important paleoceanographic event to affect Pacific seawater over the last 10 my (e.g. Abouchami et al., 1997). An effective barrier preventing direct exchange of Atlantic and Pacific water is thought to have existed by ~8 my ago (Collins et al., 1996), although exchange was not completely cut off until ~3 my ago (Keigwin, 1979, 1982). Circulation models indicate that constriction of the Panama Straits would result in increased NADW production, and it has been suggested that early NADW production might have resulted from progressive closure between 10 and 7 my ago (Maier-Reimer et al., 1990). This coincides with the initial gradual increase in SEPR molar P/Fe ratios at this time (Fig. 8). Furthermore, carbon isotope and sand fraction records from Caribbean sediments indicate that continued closure of the gateway caused a marked intensification of NADW production at ~4.6 my ago (Haug and Tiedemann, 1998). This apparently continued over the next million years, and is consistent with an overal rapid increase in molar P/Fe ratios at Site 598 between 4.6 and 3.6 my ago (Fig. 8). The nature of the observed increase in molar P/Fe ratios between 10 and 3 my ago (Fig. 8) would therefore appear broadly consistent with the proposed enhancement of NADW production (and hence increased P inputs to the deep Pacific) in response to gradual closure of the Panama gateway.

Nd and Pb isotope compositions in ferromanganese crusts and nodules then suggest an overall reduction of NADW export (see Frank et al., 2002) since the onset of Northern Hemisphere Glaciation (NHG) ~2.7 my ago, but with high overall production intensity in the following Pleistocene (Wold, 1994). The molar P/Fe data also show high overall ratios over the last 2.7 my (Fig. 8), but consistent with the overall reduction of NADW export, also show an initial rapid decrease after the onset of NHG, and an overall decrease from 0.077 ± 0.001 at 2.7–3.1 my to 0.069 ± 0.002 at 0–0.4 my. The reason for the sharp rise and subsequent decline in molar P/Fe ratios from 1.6 to 0.3 my ago (with a maximum at ~0.8 my ago) is unclear, but may relate to changes in NADW production associated with the mid-Pleistocene revolution (MPR). The MPR represents the interval when the dominant periodicity of glacial-interglacial cycles changed from the 41-kyr obliquity signal to the 100-kyr eccentricity signal (Berger and Jansen, 1994). Although the exact timing is uncertain, the MPR occurred between 1.2 and 0.6 my ago (e.g. Pisias and Moore, 1981; Raymo et al., 1989; Ruddiman et al., 1989), and may have been associated with changes in NADW production. In particular, Raymo et al. (1997) found that NADW production was suppressed between 0.95 and 0.35 my ago, which coincides with a marked decrease in molar P/Fe ratios (Fig. 8). Although studies of other Fe oxide-rich hydrothermal sediments are clearly required in order to substantiate possible relationships between changes in ocean circulation and molar P/Fe ratios, the above observations imply that these sediments may in fact be documenting a remarkable record of relative changes in SEPR deep water dissolved P concentrations.

In summary, the geochemistry of SEPR hydrothermal particles has likely been affected by temporal changes in dissolved P concentrations, although processes such as pyrite oxidation and the possible loss of a fraction of the scavenged P during diagenesis may also potentially affect molar P/Fe ratios. However, the processes responsible for these modifications are complex and poorly understood, as is their relative importance. Further detailed studies of the co-diagenesis of Fe and P beneath well-characterised plume particles are clearly required before the potential of the molar P/Fe ratio to accurately record paleoseawater P concentrations can be fully realised. However, this study suggests that the molar P/Fe ratio of oxic hydrothermal sediments may, at the very least, prove to be a useful tool for identifying relative temporal changes in deep sea phosphate concentrations.

4. Conclusions

Distal sediments deposited at ~19°S on the SEPR are enriched in hydrothermal Fe (oxyhydr)oxides and scavenged oceanic P. During diagenesis, primary ferrihydrite precipitates are partially transformed to the more stable mineral form of goethite, and to a lesser extent to clay minerals, with the result that scavenged P is extensively released to solution. A significant proportion of this P (at least 50–60%) is retained within the sediment, as authigenic apatite, by coprecipitation with secondary goethite, or by readsorption onto Fe (oxyhydr)oxides.

Molar P/Fe ratios are significantly lower than in freshly precipitated SEPR plume particles, and decrease to a sediment depth of ~12 m. Below this depth relatively constant molar P/Fe ratios are observed until a depth of ~35 m, where the ratios become highly variable. The Fe and P speciation data suggest that these trends can not be explained solely by loss of scavenged P to the overlying water column following ferrihydrite dissolution during diagenesis. Instead, changes in dissolved P off the SEPR over the last 10 my, possibly as a result of nutrient redistribution in response to changes in ocean circulation, appear to exert a major control on molar P/Fe ratios. Furthermore, we cannot discount the possibility that pyrite oxidation following deposition may contribute to the relatively low molar P/Fe ratios observed throughout these sediments. This study suggests that the molar P/Fe ratio of oxic, Fe-rich sediments may have significant potential for the determination of paleoseawater phosphate concentrations, particularly if Fe sulfide minerals are not an important component during transport and deposition.

Acknowledgments

We would like to express our gratitude to Bob Berner who, in addition to his many outstanding scientific contributions, has also inspired and tutored a generation of students and postdocs. As testament to Bob's continuing scientific legacy, many of these 'Berner kids' have themselves subsequently nurtured an array of young scientific 'hopefuls', and in this regard SWP particularly acknowledges the support of Rob Raiswell, Mike Krom and Don Canfield. This work was supported by a Marie Curie Individual Fellowship (HPMF-CT-2002-01569) awarded to S.W.P., and the Danish National Research Foundation (Danish Grundforskningsfond). We thank Jerry Bode of the ODP West Coast Repository for sampling assistance and Daniela Schmidt for helpful discussions. Alfonso Mucci, Gabriel Filippelli and two anonymous reviewers are thanked for helpful comments.

Associate editor: Alfonso Mucci

Appendix A

See Table A.1.

Table A.1

Depth (cm)	Age (my)	FeT (wt%)	Fe_{HFO} (wt%)	Fe_{goe} (wt%)	Fe_{sil} (wt%)	$CaCO_3$ (wt%)	Organic C (wt%)
Site 598							
0.5	0.01	1.27	0.53	0.58	0.16	92.8	0.07
2.5	0.05	1.17	0.45	0.58	0.14	89.7	0.05
4.5	0.09	1.07	0.38	0.56	0.13	92.6	0.04
6.5	0.13	1.10	0.41	0.55	0.14	94.2	0.03
8.5	0.17	1.32	0.46	0.67	0.19	88.1	0.03
14.5	0.29	1.80	0.58	0.93	0.29	84.9	0.03
21.0	0.42	2.59	0.81	1.48	0.30	82.9	0.03
26.5	0.53	2.82	0.87	1.56	0.39	81.7	0.04
34.5	0.69	3.86	1.03	2.24	0.59	78.1	0.05
42.5	0.85	5.55	1.49	3.52	0.54	65.7	0.05
46.5	0.93	7.00	1.76	4.35	0.89	61.8	0.07
52.5	1.05	6.51	1.64	4.13	0.74	68.3	0.08
58.5	1.17	7.10	1.76	4.59	0.75	63.4	0.06
68.5	1.37	8.10	1.85	5.18	1.07	62.0	0.04
76.5	1.53	8.07	1.62	5.52	0.93	61.3	0.05
84.5	1.69	8.38	1.70	5.59	1.09	60.1	0.05
92.5	1.85	7.72	1.51	5.05	1.16	65.0	0.06
101.0	2.01	6.27	1.21	4.17	0.89	71.3	0.04
110.5	2.10	4.35	0.88	2.94	0.53	80.6	0.03
121.5	2.20	4.28	0.82	3.01	0.45	81.1	0.03
130.5	2.28	2.96	0.66	1.98	0.32	85.9	0.02
138.5	2.35	2.45	0.51	1.70	0.24	88.3	0.03
150.5	2.46	3.15	0.62	2.15	0.38	87.1	0.02
156.5	2.51	4.06	0.74	2.69	0.63	82.8	0.02
166.5	2.61	3.09	0.59	1.97	0.53	88.8	0.01
176.5	2.70	4.55	0.78	3.13	0.64	82.9	0.02
186.5	2.79	3.98	0.74	2.79	0.45	83.9	0.02
196.5	2.88	4.71	0.78	3.22	0.71	82.7	0.02
206.5	2.97	7.10	1.13	5.26	0.71	68.9	0.03
216.5	3.06	10.26	1.38	7.71	1.17	60.8	0.05
227.5	3.16	14.26	1.87	11.31	1.08	42.8	0.04
236.5	3.24	14.53	1.81	11.57	1.15	43.6	0.08
246.5	3.33	14.15	1.63	11.44	1.08	42.8	0.07
256.5	3.42	13.32	1.63	10.26	1.43	44.6	0.03
266.5	3.51	12.15	1.58	9.28	1.29	56.0	0.05
277.5	3.61	9.82	1.44	7.57	0.81	63.9	0.04
286.5	3.70	6.55	1.00	5.17	0.38	75.7	0.03
296.5	3.79	4.86	0.74	3.71	0.41	82.3	0.01
306.5	3.88	2.97	0.54	2.41	0.02	89.3	0.06
326.5	4.06	2.72	0.46	2.05	0.21	92.3	0.01
347.5	4.25	6.24	0.95	4.57	0.72	79.0	0.02
367.5	4.43	7.83	1.13	5.95	0.75	72.9	0.04
386.5	4.61	3.34	0.54	2.54	0.26	87.4	0.02
398.5	4.71	2.60	0.43	1.73	0.44	90.1	0.01
424.5	4.95	2.51	0.52	2.02	−0.03	85.8	0.01
440.5	5.10	1.65	0.32	1.29	0.04	92.0	0.02
474.5	5.26	2.85	0.56	2.06	0.22	89.3	0.04
499.5	5.35	9.09	2.10	6.81	0.18	68.5	0.06
549.5	5.51	1.68	0.31	1.33	0.04	93.6	0.01
599.5	5.68	2.65	0.50	1.98	0.17	89.6	0.02
Site 599							
0.5	0.01	2.41	0.59	0.95	0.87	93.2	<0.01
2.5	0.05	2.84	0.75	1.76	0.33	91.6	<0.01
4.5	0.09	1.88	0.67	1.05	0.16	93.7	<0.01
6.5	0.12	1.55	0.57	0.84	0.13	94.1	<0.01
8.5	0.16	1.66	0.50	0.91	0.25	93.8	<0.01
Site 600							
0.5	0.002	1.11	0.51	0.40	0.19	94.8	<0.01
2.5	0.010	0.89	0.41	0.43	0.05	95.6	<0.01
4.5	0.018	0.92	0.43	0.43	0.06	96.1	<0.01
6.5	0.026	0.93	0.43	0.46	0.05	95.8	<0.01
8.5	0.034	0.93	0.44	0.46	0.04	95.6	<0.01

Table A.1 (*continued*)

Depth (cm)	P_{tot} (wt%)	P_{ex} (wt%)	P_{Fe} (wt%)	P_{aut} (wt%)	P_{det} (wt%)	P_{org} (wt%)	P_{bio} (wt%)	P_{HFO} (wt%)	P_{goe} (wt%)
Site 598									
0.5	0.066	0.002	0.018	0.045	0.002	0.0010	0.002	0.017	0.001
2.5	0.060	0.002	0.020	0.036	0.001	0.0007	0.002	0.018	0.002
4.5	0.063	0.003	0.015	0.033	0.001	0.0066	0.001	0.014	0.001
6.5	0.063	0.002	0.031	0.036	0.001	0.0007	0.001	0.018	0.013
8.5	0.063	0.002	0.022	0.040	0.001	0.0012	0.002	0.016	0.005
14.5	0.085	0.003	0.028	0.053	0.001	0.0008	0.002	0.017	0.011
21.0	0.131	0.003	0.037	0.081	0.003	0.0008	0.002	0.032	0.004
26.5	0.136	0.002	0.036	0.081	0.007	0.0013	0.001	0.034	0.002
34.5	0.204	0.002	0.058	0.119	0.007	0.0016	0.002	0.046	0.012
42.5	0.291	0.002	0.056	0.220	0.007	0.0029	0.002	0.040	0.017
46.5	0.383	0.002	0.090	0.251	0.005	0.0045	0.002	0.073	0.018
52.5	0.314	0.002	0.086	0.201	0.006	0.0030	0.002	0.048	0.038
58.5	0.376	0.003	0.092	0.257	0.008	0.0031	0.002	0.058	0.034
68.5	0.422	0.003	0.117	0.279	0.008	0.0027	0.002	0.034	0.083
76.5	0.401	0.004	0.112	0.259	0.010	0.0024	0.002	0.028	0.084
84.5	0.391	0.003	0.113	0.250	0.007	0.0032	0.002	0.039	0.074
92.5	0.352	0.003	0.114	0.212	0.013	0.0021	0.002	0.028	0.087
101.0	0.270	0.004	0.086	0.161	0.015	0.0010	0.002	0.036	0.051
110.5	0.212	0.003	0.054	0.136	0.012	0.0007	0.002	0.036	0.018
121.5	0.206	0.004	0.048	0.124	0.002	0.0006	0.002	0.033	0.015
130.5	0.143	0.002	0.035	0.076	0.009	0.0007	0.002	0.024	0.011
138.5	0.124	0.002	0.030	0.081	0.002	0.0007	0.001	0.021	0.009
150.5	0.153	0.003	0.041	0.075	0.006	0.0004	0.001	0.027	0.014
156.5	0.179	0.002	0.059	0.087	0.011	0.0010	0.001	0.036	0.023
166.5	0.139	0.002	0.039	0.074	0.009	0.0010	0.002	0.030	0.009
176.5	0.201	0.002	0.051	0.137	0.011	0.0013	0.002	0.030	0.021
186.5	0.196	0.003	0.049	0.113	0.011	0.0006	0.002	0.027	0.023
196.5	0.226	0.002	0.054	0.097	0.011	0.0010	0.002	0.041	0.013
206.5	0.343	0.002	0.093	0.155	0.010	0.0019	0.002	0.057	0.036
216.5	0.465	0.003	0.134	0.147	0.013	0.0026	0.002	0.087	0.047
227.5	0.619	0.003	0.185	0.262	0.016	0.0035	0.002	0.071	0.114
236.5	0.625	0.002	0.204	0.347	0.012	0.0049	0.002	0.052	0.151
246.5	0.613	0.002	0.202	0.353	0.012	0.0094	0.002	0.046	0.156
256.5	0.576	0.003	0.170	0.301	0.014	0.0033	0.002	0.050	0.120
266.5	0.494	0.003	0.165	0.328	0.014	0.0030	0.002	0.037	0.128
277.5	0.476	0.002	0.130	0.298	0.013	0.0026	0.001	0.039	0.091
286.5	0.389	0.002	0.081	0.262	0.012	0.0015	0.001	0.020	0.060
296.5	0.233	0.002	0.062	0.115	0.013	0.0007	0.002	0.045	0.017
306.5	0.140	0.002	0.040	0.088	0.005	0.0016	0.003	0.025	0.015
326.5	0.126	0.002	0.036	0.068	0.008	0.0004	0.001	0.030	0.006
347.5	0.268	0.002	0.073	0.140	0.012	0.0013	0.001	0.036	0.038
367.5	0.297	0.001	0.059	0.157	0.009	0.0008	0.002	0.018	0.041
386.5	0.138	0.002	0.038	0.072	0.006	0.0004	0.001	0.025	0.013
398.5	0.114	0.002	0.030	0.055	0.007	0.0008	0.001	0.022	0.008
424.5	0.105	0.002	0.030	0.060	0.005	0.0001	0.001	0.020	0.011
440.5	0.070	0.001	0.017	0.041	0.004	0.0001	0.001	0.009	0.008
474.5	0.101	0.001	0.015	0.056	0.002	0.0001	0.002	0.010	0.005
499.5	0.346	0.001	0.057	0.190	0.001	0.0003	0.002	0.032	0.025
549.5	0.056	0.001	0.015	0.035	0.002	0.0001	0.001	0.006	0.009
599.5	0.098	0.001	0.020	0.058	0.002	0.0001	0.001	0.008	0.012
Site 599									
0.5	0.093	0.004	0.038	0.047	0.005	0.0001	0.001	0.025	0.014
2.5	0.111	0.004	0.036	0.076	0.007	0.0001	0.001	0.009	0.027
4.5	0.104	0.004	0.039	0.063	0.009	0.0003	0.001	0.009	0.030
6.5	0.074	0.004	0.035	0.039	0.007	0.0001	0.001	0.025	0.010
8.5	0.054	0.003	0.030	0.033	0.006	0.0001	0.001	0.029	0.001
Site 600									
0.5	0.032	0.003	0.024	0.015	0.005	0.0001	0.001	0.014	0.009
2.5	0.030	0.004	0.017	0.018	0.005	0.0001	0.001	0.011	0.006
4.5	0.032	0.004	0.023	0.016	0.002	0.0001	0.001	0.016	0.008
6.5	0.055	0.004	0.028	0.025	0.005	0.0001	0.001	0.017	0.026
8.5	0.043	0.004	0.026	0.016	0.005	0.0001	0.001	0.014	0.012

References

Abouchami, W., Goldstein, S.L., Galer, S.J.G., Eisenhauer, A., Mangini, A., 1997. Secular changes of lead and neodymium in central Pacific seawater recorded by a Fe–Mn crust. *Geochim. Cosmochim. Acta* **61**, 3957–3974.

Baker, E.T., Lavelle, J.W., Massoth, G.J., 1985. Hydrothermal particle plumes over the southern Juan de Fuca Ridge. *Nature* **316**, 342–344.

Berger, W.H., Jansen, E., 1994. Mid-Pleistocene climate shift: the Nansen connection. In: Johannesses, O.M., Muench, R.D., Overland, J.E. (Eds.) *The Polar Oceans and Their Role in Shaping the Global Environment: The Nansen Centennial Volume, AGU, Geophys. Monog.*, **85**, 295–312.

Berner, R.A., 1973. Phosphate removal from sea water by adsorption on volcanogenic ferric oxides. *Earth Planet. Sci. Lett.* **18**, 77–86.

Bertram, M.A., Cowen, J.P., Thomson, R.E., Feely, R.A., 2002. Compositional variability in the ascending fluxes from a hydrothermal plume. *J. Geophys. Res.* **107**, 3191. doi:10.1029/2000JC000223.

Bjerrum, C.J., Canfield, D.E., 2002. Ocean productivity before about 1.9 Gyr ago limited by phosphorus adsorption onto iron oxides. *Nature* **417**, 159–162.

Bloomstine, M.K., Rea, K.R., 1986. Post-middle Oligocene eolian deposition from the trade winds of the southeast Pacific. *Initial Reports of the Deep Sea Drilling Project* **92**, 331–340.

Bower, A.S., Le Cann, B., Rossby, T., Zenk, W., Gould, J., Speer, K., Richardson, P.L., Prater, M.D., Zhang, H.-M., 2002. Directly measured mid-depth circulation in the northeastern North Atlantic Ocean. *Nature* **419**, 603–607.

Broeker, W.S., Peng, T.H., 1982. Tracers in the Sea. Lamont-Doherty Earth Obs., Palisades, New York.

Canfield, D.E., 1998. A new model for Proterozoic ocean chemistry. *Nature* **396**, 450–453.

Cave, R.R., German, C.R., Thomson, J., Nesbitt, R.W., 2002. Fluxes to sediments underlying the Rainbow hydrothermal plume at 36°14′N on the Mid-Atlantic Ridge. *Geochim. Cosmochim. Acta* **66**, 1905–1923.

Collins, L.S., Coates, A.G., Berggren, W.A., Aubry, M.P., Zhang, J., 1996. The late Miocene Panama isthmian strait. *Geology* **24**, 687–690.

Cornell, R.M., Schwertmann, U., 1996. *The Iron Oxides: Structure, Properties, Reactions, Occurrence and Uses*. VCH, Weinheim, Germany.

Curtis, C.D., 1985. Clay mineral precipitation and transformation during burial diagenesis. *Phil. Trans. R. Soc. Lond.* **315**, 91–105.

Delaney, M.L., Filippelli, G.M., 1994. An apparent contradiction in the role of phosphorus in Cenozoic chemical mass balances for the world ocean. *Paleoceanography* **9**, 513–527.

Douville, E., Charlou, J.L., Oelkers, E.H., Bienvenu, P., Jove Colon, C.F., Donval, J.P., Fouquet, Y., Prieur, D., Appriou, P., 2002. The rainbow vent fluids (36°14′N, MAR): the influence of ultramafic rocks and phase separation on trace metal content in Mid-Atlantic Ridge hydrothermal fluids. *Chem. Geol.* **184**, 37–48.

Dymond, J., 1981. The geochemistry of Nazca Plate sediments: an evaluation of hydrothermal, biogenic, detrital and hydrogenous sources. *Geol. Soc. Am. Mem.* **154**, 133–173.

Edmonds, H.N., German, C.R., 2004. Particle geochemistry in the Rainbow hydrothermal plume, Mid-Atlantic Ridge. *Geochim. Cosmochim. Acta* **68**, 759–772.

Eijsink, L.M., Krom, M.D., Herut, B., 2000. Speciation and burial flux of phosphorus in the surface sediments of the eastern Mediterranean. *Am. J. Sci.* **300**, 483–503.

Feely, R.A., Lewison, M.A., Massoth, G.J., Baldo, R.G., Lavelle, J.W., Byrne, R.H., Von Damm, K.L., Curl Jr., H.C., 1987. Composition and dissolution of black smoker particles from active vents on the Juan de Fuca Ridge. *J. Geophys. Res.* **92**, 11347–11363.

Feely, R.A., Geiselman, T.L., Baker, E.T., Massoth, G.J., Hammond, S.R., 1990a. Distribution and composition of buoyant and non-buoyant hydrothermal plume particles from the ASHES vent at Axial Volcano, Juan de Fuca Ridge. *J. Geophys. Res.* **95**, 12855–12874.

Feely, R.A., Massoth, G.J., Baker, E.T., Cowen, J.P., Lamb, M.F., Krogslund, K.A., 1990b. The effect of hydrothermal processes on midwater phosphorus distributions in the northeast Pacific. *Earth Planet. Sci. Lett.* **96**, 305–318.

Feely, R.A., Trefry, J.H., Massoth, G.J., Metz, S., 1991. A comparison of the scavenging of phosphorus and arsenic from seawater by hydrothermal iron oxyhydroxides in the Atlantic and Pacific Oceans. *Deep-Sea Res.* **38**, 617–623.

Feely, R.A., Massoth, G.J., Baker, E.T., Lebon, G.T., Geiselman, T., 1992. Tracking the dispersal of hydrothermal plumes from the Juan de Fuca Ridge using suspended matter compositions. *J. Geophys. Res.* **97**, 3457–3468.

Feely, R.A., Massoth, G.J., Trefry, J.H., Baker, E.T., Paulson, A.J., Lebon, G.T., 1994. Composition and sedimentation of hydrothermal plume particles from North Cleft segment, Juan de Fuca Ridge. *J. Geophys. Res.* **99**, 4985–5006.

Feely, R.A., Baker, E.T., Marumo, K., Urabe, T., Ishibashi, J., Gendron, J., Lebon, G.T., Okamura, K., 1996. Hydrothermal plume particles and dissolved phosphate over the superfast-spreading southern East Pacific Rise. *Geochim. Cosmochim. Acta* **60**, 2297–2323.

Feely, R.A., Trefry, J.H., Lebon, G.T., German, C.R., 1998. The relationship between P/Fe and V/Fe ratios in hydrothermal precipitates and dissolved phosphate in seawater. *Geophys. Res. Lett.* **25**, 2253–2256.

Filippelli, G.M., Delaney, M.L., 1994. The oceanic phosphorus cycle and continental weathering during the Neogene. *Paleoceanography* **9**, 643–652.

Filippelli, G.M., Delaney, M.L., 1996. Phosphorus geochemistry of equatorial Pacific sediments. *Geochim. Cosmochim. Acta* **60**, 1479–1495.

Fitzpatrick, R.W., Le Roux, J., Schwertmann, U., 1978. Amorphous and crystalline titanium and iron-titanium oxides in synthetic preparations, at near ambient conditions, and in soil clays. *Clays Clay Miner.* **26**, 189–201.

Frank, M., Whiteley, N., Kasten, S., Hein, J.R., O'Nions, K., 2002. North Atlantic Deep Water export to the Southern Ocean over the past 14 Myr: evidence from Nd and Pb isotopes in ferromanganese crusts. *Paleoceanography*, 17. doi:10.1029/2000PA000606.

Froelich, P.N., Bender, M.L., Luedtke, N.A., Heath, G.R., DeVries, T., 1982. The marine phosphorus cycle. *Am. J. Sci.* **282**, 474–511.

Föllmi, K.B., 1995. 160 m.y. record of marine sedimentary phosphorus burial: coupling of climate and continental weathering under greenhouse and icehouse conditions. *Geology* **23**, 859–862.

German, C.R., Klinkhammer, G.P., Edmond, J.M., Mitra, A., Elderfield, H., 1990. Hydrothermal scavenging of rare earth elements in the ocean. *Nature* **345**, 516–518.

German, C.R., Campbell, A.C., Edmond, J.M., 1991. Hydrothermal scavenging at the Mid-Atlantic Ridge: modification of trace element dissolved fluxes. *Earth Planet. Sci. Lett.* **107**, 101–114.

Gieskes, J.M., Boulégue, J., 1986. Interstital water studies, Leg 92. *Initial Reports of the Deep Sea Drilling Project* **92**, 423–429.

Haug, G.H., Tiedemann, R., 1998. Effect of the formation of the Isthmus of Panama on Atlantic Ocean thermohaline circulation. *Nature* **393**, 673–676.

Ishibashi, J., Wakita, H., Okamura, K., Nakayama, E., Feely, R.A., Lebon, G.T., Baker, E.T., Marumo, K., 1997. Hydrothermal methane and manganese variation in the plume over the superfast-spreading southern East Pacific Rise. *Geochim. Cosmochim. Acta* **61**, 485–500.

Kastner, M., 1986. Mineralogy and diagenesis of sediments at site 597: preliminary results. *Initial Reports of the Deep Sea Drilling Project* **92**, 345–349.

Keigwin, L.D.J., 1979. Late Cenozoic stable isotope stratigraphy and paleoceanography of DSDP sites from the East Equatorial and Central North Pacific Ocean. *Earth Planet. Sci. Lett.* **45**, 361–382.

Keigwin, L.D.J., 1982. Isotopic paleoceanography of the Caribbean and east Pacific: role of Panama uplift in Late Neogene times. *Science* **217**, 350–355.

Kennedy, C.B., Scott, S.D., Ferris, F.G., 2004. Hydrothermal phase stabilization of 2-line ferrihydrite by bacteria. *Chem. Geol.* **212**, 269–277.

Klinkhammer, G., Hudson, A., 1986. Dispersal patterns for hydrothermal plumes in the South-Pacific using manganese as a tracer. *Earth Planet. Sci. Lett.* **79**, 241–249.

Koroleff, F., 1976. Determination of nutrients. In: Grasshoff, K., Ehrhardt, M., Kremling, K. (Eds.), *Methods of Seawater Analysis*. Verlag-Chimie, Berlin, p. 117.

Ku, T.C.W., Walter, L.M., 2003. Syndepositional formation of Fe-rich clays in tropical shelf sediments, San Blas Archipelago, Panama. *Chem. Geol.* **197**, 197–213.

Kyte, T.T., Leinen, M., Heath, G.R., Zouh, L., 1993. Cenozoic sedimentation history of the central North Pacific: inferences from the elemental geochemistry of core LL44-GPC3. *Geochim. Cosmochim. Acta* **57**, 1719–1740.

Leinen, M., 1986. Calcium carbonate sedimentation at the subtropical south Pacific drill sites from Leg 92 and the carbonate stratigraphy of site 598: preliminary studies. *Initial Reports of the Deep Sea Drilling Project* **92**, 305–330.

Lourens, L.J., Hilgen, F.J., Laskar, J., Shackleton, N.J., Wilson, D., 2004. The Neogene Period. In: Gradstein, F.M., Ogg, J., Smith, A.G. (Eds.), *A Geologic Time Scale 2004*. Cambridge University Press, Cambridge.

Lucotte, M., Mucci, A., Hillaire-Marcel, C., Trom, S., 1994. Early diagenetic processes in deep Labrador Sea sediments: reactive and nonreactive iron and phosphorus. *Can. J. Earth Sci.* **31**, 14–27.

Lupton, J.E., Craig, H., 1981. A major helium-3 source at 15°S on the East Pacific Rise. *Science* **214**, 13–18.

Lupton, J.E., Baker, E.T., Garfield, N., Massoth, G.J., Feely, R.A., Cowen, J.P., Greene, R.R., Rago, T.A., 1998. Tracking the evolution of a hydrothermal event plume with a RAFOS neutrally buoyant drifter. *Science* **280**, 1052–1055.

Lyle, M.W., 1986. Major element composition of Leg 92 sediments. *Initial Reports of the Deep Sea Drilling Project* **92**, 355–370.

Lyle, M.W., Owen, R.M., Leinen, M., 1986. History of hydrothermal sedimentation at the East Pacific Rise, 19°S. *Initial Reports of the Deep Sea Drilling Project* **92**, 585–596.

Maier-Reimer, E., Mikolajewicz, U., Crowley, T.J., 1990. Ocean general circulation model sensitivity experiment with an open Central American isthmus. *Paleoceanography* **5**, 349–366.

Marchig, V., Gundlach, H., 1982. Iron-rich metalliferous sediments on the East Pacific Rise: prototype of undifferentiated metalliferous sediments on divergent plate boundaries. *Earth Planet. Sci. Lett.* **58**, 361–382.

Marchig, V., Erzinger, J., 1986. Chemical composition of Pacific sediments near 20°S: changes with increasing distance from the East Pacific Rise. *Initial Reports of the Deep Sea Drilling Project* **92**, 371–381.

Metz, S., Trefry, J.H., 1993. Field and laboratory studies of metal uptake and release by hydrothermal precipitates. *J. Geophys. Res.* **98**, 9661–9666.

Michalopoulos, P., Aller, R.C., 1995. Rapid clay mineral formation in Amazon delta sediments: reverse weathering and oceanic elemental cycles. *Science* **270**, 614–617.

Mottl, M.J., McConachy, T.F., 1990. Chemical processes in buoyant hydrothermal plumes on the East Pacific Rise near 21°N. *Geochim. Cosmochim. Acta* **54**, 1911–1927.

Olivarez, A.M., Owen, R.M., 1989. REE/Fe variations in hydrothermal sediments: Implications for the REE content of seawater. *Geochim. Cosmochim. Acta* **53**, 757–762.

Pisias, N.G., Moore, T.C., 1981. The evolution of Pleistocene climate: a time series approach. *Earth Planet. Sci. Lett.* **52**, 450–456.

Poulton, S.W., Raiswell, R., 2002. The low-temperature geochemical cycle of iron: from continental fluxes to marine sediment deposition. *Am. J. Sci.* **302**, 774–805.

Poulton, S.W., Canfield, D.E., 2005. Development of a sequential extraction procedure for iron: implications for iron partitioning in continentally derived particulates. *Chem. Geol.* **214**, 209–221.

Raymo, M.E., 1994. The Himalayas, organic carbon burial, and climate in the Miocene. *Paleoceanography* **9**, 399–404.

Raymo, M.E., Ruddiman, W.F., 1992. Tectonic forcing of late Cenozoic climate. *Nature* **359**, 117–122.

Raymo, M.E., Ruddiman, W.F., Backman, J., Clement, B.M., Martinson, D.G., 1989. Late Pliocene variation in northern hemisphere ice sheets and North Atlantic deep water circulation. *Paleoceanography* **4**, 413–446.

Raymo, M.E., Oppo, D.W., Curry, W., 1997. The mid-Pleistocene climate transition: a deep sea carbon isotope perspective. *Paleoceanography* **12**, 546–559.

Reid, J.L., 1982. Evidence of an effect of heat flux from the East Pacific Rise upon the characteristics of the mid-depth waters. *Geophys. Res. Lett.* **9**, 381–384.

Reid, J.L., Lynn, R.J., 1971. On the influence of the Norwegian-Greenland and Weddell Seas upon the bottom waters of the Indian and Pacific oceans. *Deep-Sea Res.* **18**, 1063–1088.

Ruddiman, W.F., Raymo, M.E.m., Martinson, D.G., Clement, B.M., Backman, J., 1989. Pleistocene evolution of Northern Hemisphere climate. *Paleoceanography* **4**, 353–412.

Rudnicki, M.D., Elderfield, H., 1993. A chemical model of the buoyant and neutrally buoyant plume above the TAG vent field, 26 degrees N, Mid-Atlantic Ridge. *Geochim. Cosmochim. Acta* **57**, 2939–2957.

Ruttenberg, K.C., 1992. Development of a sequential extraction method for different forms of phosphorus in marine sediments. *Limnol. Oceanogr.* **37**, 1460–1482.

Ruttenberg, K.C., 1993. Reassessment of the oceanic residence time of phosphorus. *Chem. Geol.* **107**, 405–409.

Ruttenberg, K.C., Berner, R.A., 1993. Authigenic apatite formation and burial in sediments from non-upwelling, continental margin environments. *Geochim. Cosmochim. Acta* **57**, 991–1007.

Schaller, T., Morford, J., Emerson, S.R., Feely, R.A., 2000. Oxyanions in metalliferous sediments: tracers for paleoseawater metal concentrations? *Geochim. Cosmochim. Acta* **63**, 2243–2254.

Schenau, S.J., De Lange, G.J., 2000. A novel chemical method to quantify fish debris in marine sediments. *Limnol. Oceanogr.* **45**, 963–971.

Schenau, S.J., Slomp, C.P., De Lange, G.J., 2000. Phosphogenesis and active phosphorite formation in sediments from the Arabian Sea oxygen minimum zone. *Mar. Geol.* **169**, 1–20.

Schwertmann, U., Murad, E., 1983. Effect of pH on the formation of goethite and hematite from ferrihydrite. *Clays Clay Miner.* **31**, 277–284.

Slomp, C.P., Thomson, J., De Lange, G.J., 2002. Enhanced regeneration of phosphorus during formation of the most recent eastern Mediterranean sapropel (S1). *Geochim. Cosmochim. Acta* **66**, 1171–1184.

Speer, K.G., Gould, J., LaCasce, J., 1999. Year-long float trajectories in the Labrador Sea water of the eastern North Atlantic Ocean. *Deep-Sea Res.* **46**, 165–179.

Trefry, J.H., Metz, S., 1989. Role of hydrothermal precipitates in the geochemical cycling of vanadium. *Nature* **342**, 531–533.

Trocine, R.P., Trefry, J.H., 1988. Distribution and chemistry of suspended particles from an active hydrothermal vent site on the Mid-Atlantic Ridge at 26°N. *Earth Planet. Sci. Lett.* **88**, 1–15.

Turekian, K.K., Wedephol, K.H., 1961. Distribution of the elements in some major units of the earth's crust. *Geol. Soc. Am. Bull.* **75**, 175–192.

Urabe, T. et al., 1995. Magmatic influence on hydrothermal activity along the superfast-spreading southern East Pacific Rise. *Science* **269**, 1092–1095.

Van der Zee, C., Slomp, C.P., van Raaphorst, W., 2002. Authigenic P formation and reactive P burial in sediments of the Nazaré canyon on the Iberian margin (NE Atlantic). *Mar. Geol.* **185**, 379–392.

Walker, S.L., Baker, E.T., 1988. Particle-size distributions within hydrothermal plumes over the Juan de Fuca Ridge. *Mar. Geol.* **78**, 217–226.

Wheat, C.G., Feely, R.A., Mottl, M.J., 1996. Phosphate removal by oceanic hydrothermal processes: an update of the phosphorus budget in the oceans. *Geochim. Cosmochim. Acta* **60**, 3593–3608.

Wold, C.N., 1994. Cenozoic sediment accumulation on drifts in the northern North Atlantic. *Paleoceanography* **9**, 917–941.

Woodruff, F., Savin, S., 1989. Miocene deepwater oceanography. *Paleoceanography* **4**, 87–140.

Wright, J.D., Miller, K.G., 1996. Control of North Atlantic Deep Water circulation by the Greenland-Scotland Ridge. *Paleoceanography* **11**, 157–170.

Yuan, G., Lavkulich, L.M., 1995. Colorimetric determination of phosphorus in citrate-bicarbonate-dithionite extracts of soils. *Community Soil Science Plant Analysis* **26**, 1979–1988.

Zhao, J., Huggins, F.E., Feng, Z., Huffman, G.P., 1994. Ferrihydrite: surface structure and its effects on phase transformation. *Clays Clay Miner.* **42**, 737–746.